

Abstract

Nitrogen-vacancy (NV) centers are defects in diamonds, which, due to their electronic structure, have been extensively studied as magnetic field sensors. Such field detection applications usually employ the NV centers to detect field components aligned with the direction of the internally-defined spin axis of the NV center. In this work we detect magnetic fields not only aligned with the NV axis but making an angle θ with it. This detection scheme clearly shows that NV centers can be used as θ^2 sensors. We further demonstrate that the sensitivity of this sensor increases very rapidly with increasing magnetic field, diverging as the external field approaches a value pre-defined by NV center's internal parameters. We show the sensitivity of this θ^2 sensor matches up perfectly with the theoretical predictions of the same, made in one of our previous works [1]. These results show that NV centers can be excellent for making quantum nondemolition (QND) measurements on systems such as a harmonic oscillator, to probe the oscillators quantum behavior.

Nitrogen Vacancy centers in diamond as θ^2 sensors

Shonali Dhingra, Brian D'Urso*

Department of Physics and Astronomy, University of Pittsburgh

1 Introduction

Nitrogen vacancy (NV) centers in diamond are naturally occurring defects in diamond, which consist of a substitutional nitrogen atom and an adjacent carbon vacancy [2]. These defects can also be artificially introduced in diamonds through irradiation and annealing [3, 4]. Owing to their ease of manipulation and readout, and long coherence times, even at room temperature, they have recently been extensively characterized and used in myriad of applications [4]. One such application of NV centers is as a sensor for dc, ac and fluctuating magnetic fields [5–10]. The work done in this regard has shown that the NV centers can be used to detect nanotesla magnetic fields with nanoscale spatial resolution [8], can be used for these purposes at room temperature [7], and an array of them can be used to map out the magnetic fields in a two-dimensional area [9]. Most of these applications choose the NV center aligned in the direction of the external magnetic field [8] or they detect the component of the magnetic field that is aligned in the direction of the NV center [6]. For the applications that do detect magnetic fields that are not aligned with the direction of the NV center have to do so by iteratively fitting parameters and minimizing error functions [9]. Due to these limitations, the maximum magnetic fields measured by such techniques gets limited to ≤ 10 mT [7, 9].

Recently, a variety of hybrid systems, involving mechanical oscillators coupled with spin systems [1, 11, 12], are being studied and used for characterization of quantum properties of their components. With the advent of such systems, a class of measurement known as quantum nondemolition (QND) is re-emerging. Since the introduction of QND measurements [13, 14], this measurement class has found use in a wide variety of physics applications such as gravitational-wave detection [15], weak force detection using harmonic oscillators [16], optics [17] etc. A QND measurement scheme allows repeated quantum measurements to be made on the system by reducing back-action of such measurements onto the system. In a previous work, we proposed a hybrid system comprising of a nanomechanical oscillator (NMO) coupled to an NV center in presence of an external magnetic field [1]. This hybrid

*Electronic address: dursobr@pitt.edu

system results in quadratic coupling between the NMO and the NV center, which allows us to use a QND measurement scheme [16] on the system to discern quantum behavior of the NMO using NV center as a probe.

The quadratic coupling in this system results from NV-containing diamond nanocrystals physically placed on top of the NMO undergoing torsional mode of oscillation. Under these conditions, in presence of an external magnetic field, the NV center gets coupled to the angle of oscillation (θ) of the NMO in a quadratic manner around $\theta = 0$ (the linear coupling is negligible in this regime). This θ^2 coupling occurs due to mixing of the spin states (S_z with S_x or S_y) of the NV centers, unlike previous works in which the S_z spin state of the NV is used to detect the component of the magnetic field along the same direction [6]. For all such schemes which involve measuring only the component of the magnetic field aligned with the direction of the NV ($\cos(\theta)$ component), the NV center can be thought of as θ^2 sensor, with its sensitivity increasing linearly with increasing the measured magnetic field. In our QND scheme, the NV center acts as a θ^2 sensor, with its sensitivity increasing much faster than linearly with the measured external magnetic field.

In this work, we demonstrate how to identify the direction of NV centers by applying an external magnetic field around them. We further use this ability to experimentally verify that the NV center is indeed a great θ^2 sensor, the sensitivity of which agrees with the theoretical predictions made in a previous work [1].

2 Theory

The energy structure of the NV center's ground state has been extensively studied [2, 4], and is understood to be as shown in Fig. 1. As can be seen from this figure, the ground state (3A) is a spin triplet, with $|0\rangle$, $|1\rangle$ and $|-1\rangle$ as eigenstates, defined in the S_z basis (along the $NV - \hat{z}$ axis), where state $|i\rangle$ has $m_s = i$. In absence of any external magnetic field, the $|1\rangle$ and $|-1\rangle$ states are degenerate, with a zero-field splitting of $\Delta = 2.87\text{ GHz}$ above the $|0\rangle$ spin state. In presence of an external magnetic field, the degeneracy between the $|1\rangle$ and $|-1\rangle$ states is lifted by amounts proportional to the external field.

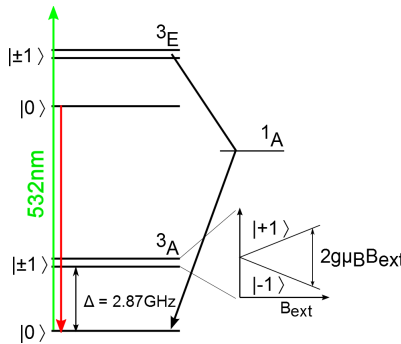


Figure 1: Energy structure of the ground state of the NV^- center.

The Hamiltonian for the ground state of the NV center can be written as [6, 18]:

$$H_{NV} = \hbar\Delta S_z^2 + g\mu_B (\vec{S} \cdot \vec{B}_{ext}) \quad (1)$$

where Δ is the zero-field splitting, $g \approx 2$ is the electron g-factor in the NV center, μ_B is the Bohr magneton, \vec{S} is the electronic spin of the NV center and \vec{B}_{ext} is the external magnetic field.

In our experiment, at any instant in time, the applied magnetic field \vec{B}_{ext} could be at an arbitrary angle with respect to the NV spin vector \vec{S} . This gives the term $\vec{S} \cdot \vec{B}_{ext}$ in Eq. 1 an angular (θ) dependence, where θ is the angle between \vec{B}_{ext} and \vec{S} . For this work, we fix the direction of the NV center, and vary the external magnetic field around on a spherical axes system. For the NMO-NV proposed hybrid system [1], we would fix the direction of magnetic field, and the direction of the NV center would move around due to the oscillation of the NMO. In either case, H_{NV} takes the following form, where we assume a 2-dimensional relative movement between \vec{B}_{ext} and \vec{S} .

$$H_{NV} = \hbar\Delta S_z^2 + g\mu_B B_{ext} (S_y \sin \theta + S_z \cos \theta) \quad (2)$$

Further analyzing the Hamiltonian of the NV center, by finding the eigenvalues of H_{NV} with θ as a parameter, we see the eigenvalues $\lambda_i(\theta)$ have the following form

$$\lambda_i(\theta) = \hbar\omega_i + \kappa_i\theta^2 + O(\theta^4) \quad (3)$$

where $i = -1, 0$, or $+1$ is a label which is equivalent to the NV center m_s when $\theta = 0$. In the θ -independent term in $\lambda_i(\theta)$, $\hbar\omega_i$ is simply the result of combining the zero field splitting with the static external field at $\theta = 0$:

$$\omega_{\pm 1} = \Delta (1 \pm B_{ext}/B_{zfs}) \quad (4)$$

$$\omega_0 = 0 \quad (5)$$

where $B_{zfs} = \hbar\Delta/g\mu_B \approx 102.5$ mT is the magnitude of the effective internal magnetic field which results in the zero field splitting Δ . As a vector, B_{zfs} can be thought of as being along the axis of the NV center. By writing the θ -independent term of the eigenvalues of H_{NV} in the above form, we can clearly see that on applying an external magnetic field, the degeneracy between $|1\rangle$ and $|-1\rangle$ states is broken, and the energy gap between $|0\rangle$ and $|-1\rangle$ decreases, and between $|0\rangle$ and $|1\rangle$ increases.

The θ^2 coefficient in $\lambda_i(\theta)$, κ_i , for the three NV spin states, namely $|0\rangle$, $|1\rangle$ and $|-1\rangle$, is:

$$\kappa_{\pm 1} = -\hbar\Delta \frac{B_{ext}}{2(B_{ext} \pm B_{zfs})} \quad (6)$$

$$\kappa_0 = \hbar\Delta \frac{B_{ext}^2}{B_{ext}^2 - B_{zfs}^2} \quad (7)$$

This gives us an analytical form for the energy gap between $|0\rangle$ and $|-1\rangle$, and $|0\rangle$ and $|+1\rangle$ spin states, near $\theta = 0$, as κ_0- and κ_0+ , respectively, as shown below:

$$\kappa_{0-} = -\hbar\Delta \frac{(B_{ext})(3B_{ext}+B_{zfs})}{2(B_{zfs}^2-B_{ext}^2)} \quad (8)$$

$$\kappa_{0+} = -\hbar\Delta \frac{(B_{ext})(3B_{ext}-B_{zfs})}{2(B_{zfs}^2-B_{ext}^2)} \quad (9)$$

The eigenvalues, $\lambda_i(\theta)$, of H_{NV} for $i = 0$ and -1 , are plotted below for three different external magnetic field values. The energy gap between these spin states is also plotted for the same magnetic field values. As can be seen from Fig 2(b), the curvature of the energy gap between spin states $|0\rangle$ and $|-1\rangle$ increases with the increase of the external magnetic field. This shows that the sensitivity of the NV center as a θ^2 sensor increases with increasing magnetic field. Also looking at the figure, one can see a sharp nonlinear dependence of the energy gap between these spin states around $\theta = 0$, which is the result of an avoided level crossing between these states when B_{ext} approaches B_{zfs} . This results in making the sensitivity of the NV center as a θ^2 sensor increase more than linearly with increasing magnetic field, and diverge when B_{ext} approaches B_{zfs} . In this work, we have tried to experimentally verify these theoretical predictions about the NV centers.

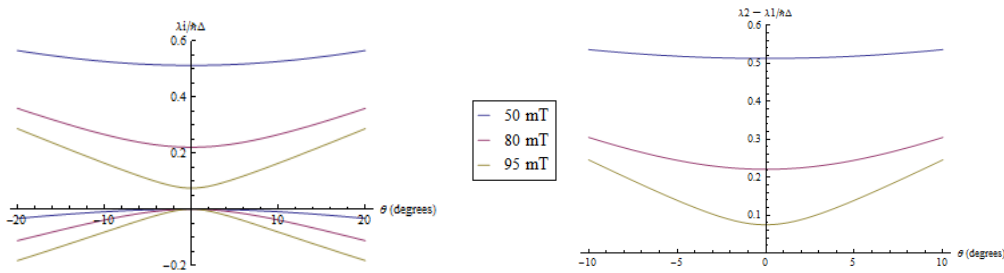


Figure 2: Considering only the $|0\rangle$ and $|-1\rangle$ spin states (a)Eigenvalues of H_{NV} at different magnetic fields and (b)Energy gap between these states at the same magnetic fields

3 Experimental Data

To verify the above-mentioned theoretical predictions, electronic spin resonance (ESR) was performed on diamond nanocrystals with NV ensembles. The nanocrystals used for this purpose were $\sim 100\text{ nm}$ in diameter and were prepared using high pressure high temperature (HPHT) techniques. We spin-coated them on a polished piece of silicon, with a density low-enough to be able to resolve individual nanodiamonds. Confocal laser scanning microscopy (CLSM) was employed to visualize and detect the fluorescence of the nanocrystals. Green laser light ($\lambda = 532\text{ nm}$) was used to excite the NV centers in these nanocrystals and their fluorescence was detected by cutting out wavelengths between 517 nm and 548 nm , using a notch filter. To drive resonant transitions between $|0\rangle$ and $|\pm 1\rangle$ spin states, a microwave (MW) drive was applied to this sample using an un-terminated loop, 2-3 mm in diameter, made out of $30\text{ }\mu\text{m}$ diameter tungsten wire. This resulted in a dip in fluorescence

at the frequency corresponding to the energy gap between the $|0\rangle$ and $|\pm 1\rangle$ spin states i.e. $\sim 2.87 \text{ GHz}$. This is the characteristic ESR signal as expected from single NV centers or NV center ensembles [4, 7, 19]. ESR signals from three such diamond nanocrystals on our sample is shown in the figure below. The breaking of the ESR dip into two dips shows the presence of strain and breaking of axial symmetry, again as expected for NV center ensembles [19].

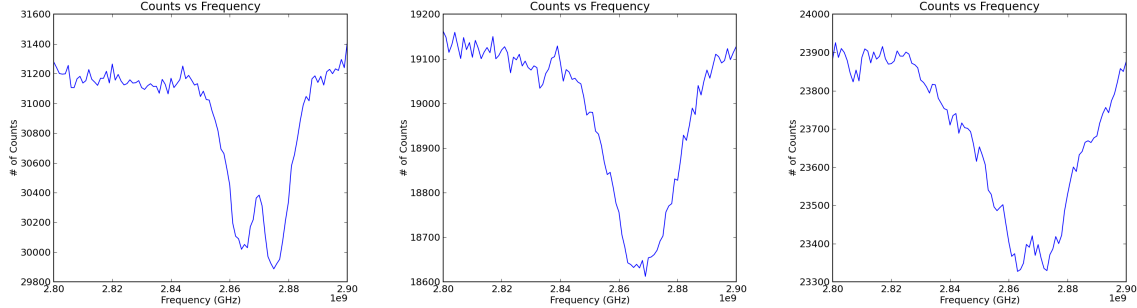


Figure 3: Optically detected ESR signal from three diamond nanocrystals, containing NV center ensembles, on our sample. All three show ESR dips $\sim 2.87 \text{ GHz}$ in absence of any external magnetic field, as expected.

To lift the degeneracy between $|\pm 1\rangle$ spin states, we applied an external magnetic field B_{ext} around our sample, using electromagnetic coils. Due to experimental limitations, $\approx \pm 100 \text{ mT}$ was available in the direction perpendicular to the sample (\hat{z}), and $\approx \pm 25 \text{ mT}$ in the two directions parallel to the sample surface (\hat{x} and \hat{y}). On a 3D plot, this accessible region of magnetic field can be thought of as a cuboid with square faces of side 25 mT and a height of $\pm 100 \text{ mT}$, as shown in Fig. 4. This cuboid-shaped region limits the accessible areas of magnetic fields with specific magnitudes, as shown by the shapes inside the cuboid. Full sphere can be accessed for $B_{ext} \leq 25 \text{ mT}$, but for $25 \text{ mT} \leq B_{ext} \leq 100 \text{ mT}$ only spherical caps are accessible, as shown in Fig. 4(a). To account for all possible NV center directions in any arbitrarily-oriented diamond nanocrystal, we can think of B_{zfs} as forming a sphere of radius 102.5 mT on the same 3D plot.

In a diamond nanocrystal, the direction of any NV center ($NV - \hat{z}$) can be in any one of the four possible orientations along the carbon tetrahedron bonds (shown in blue arrows in Fig. 4). Due to the symmetry between $|1\rangle$ and $|-1\rangle$ spin states, the $NV - \hat{z}$ direction could also be the four orientations directly opposite to the carbon tetrahedron bonds (shown in red arrows in Fig. 4). The direction of the $NV - \hat{z}$ also being the direction of B_{zfs} , suggests that for any arbitrary diamond nanocrystal, there are eight possible directions where B_{zfs} and B_{ext} could align with each other. These eight directions define the orientations along which the NV centers could behave as θ^2 sensors.

Our first experimental goal for this work, was to recognize these $NV - \hat{z}$ orientations for any randomly-picked diamond nanocrystal. For this purpose we swept B_{ext} only in the $+\hat{z}$ direction along hemispheres/spherical caps shown in Fig. 4(a). This would suffice due to the mirror symmetry about the XY-plane of B_{ext} and the NV centers. On applying an external

magnetic field, the $|1\rangle$ and $| -1\rangle$ spin states undergo Zeeman splitting, as shown in Fig. 1. Thus the ESR dip, which occurs due to resonant transitions between $|0\rangle$ and $|\pm 1\rangle$ spin states at MW frequencies corresponding to the energy difference between these states, splits into two dips, as expected. Due to the decrease in energy gap between $|0\rangle$ and $| -1\rangle$, and increase in energy gap between $|0\rangle$ and $|1\rangle$, the corresponding ESR dips are expected to decrease and increase in frequency respectively from 2.87 GHz , on increasing the magnitude of B_{ext} . For our purposes, we monitored the ESR dip corresponding to the energy gap between $|0\rangle$ and $| -1\rangle$. The ESR dip shift is expected to be linear in frequency with increasing B_{ext} , if the direction of B_{ext} is aligned with the $NV - \hat{z}$ direction.

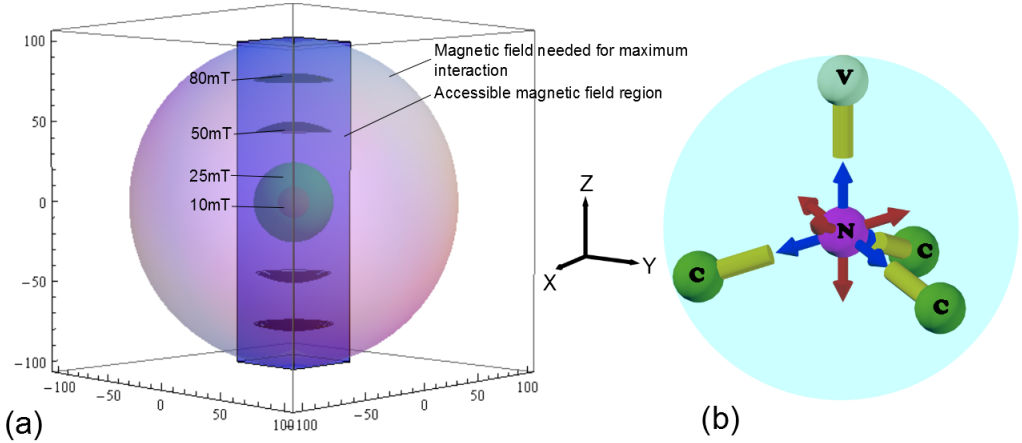


Figure 4: Pictorial 3D representation of accessible external magnetic field (B_{ext}) and possible NV center orientations (directions of B_{zfs}) in any arbitrary diamond nanocrystal (a) The pink sphere represents the direction of possible B_{zfs} for all diamond nanocrystals. The cuboid with square faces of side 25 mT and a height of $\pm 100\text{ mT}$ represents the experimentally accessible magnetic field region, along the experimentally defined \hat{z} direction of B_{ext} . This cuboid-shaped region limits the accessible areas of magnetic fields with specific magnitudes, as shown by the shapes inside the cuboid. (b) A carbon tetrahedron structure in any arbitrary diamond nanocrystal is shown. Assuming the nitrogen atom is at the center of the tetrahedron (pink), and one of the other carbon atom (green) sites is vacant (light green), the $NV - \hat{z}$ direction could be in one of four possible orientations (shown in blue arrows). Due to the symmetry between $|1\rangle$ and $| -1\rangle$ spin states, the $NV - \hat{z}$ direction could also be the four orientations opposing the carbon tetrahedron bonds (shown in red arrows). Thus for any arbitrary diamond nanocrystal, there are eight possible directions where B_{zfs} and B_{ext} could align with each other defining the orientations along which the NV centers could behave as θ^2 sensors.

We monitored the ESR dip depth and frequency location while sweeping a fixed magnitude of B_{ext} around in azimuthal and polar angles about the \hat{z} direction. These plots for a diamond nanocrystal which was $\approx 10\text{ }\mu\text{m}$ away from the edge of the microwave loop are shown in Fig. 5. Similar behavior was observed in other diamond nanocrystals within $20\text{--}30\text{ }\mu\text{m}$ of microwave loop. The colormap for these plots is also shown. Fig. 5(a) and Fig. 5(b)

show the behavior of the ESR dip depth and dip location respectively, while sweeping 20 mT magnetic field on a hemisphere. Such plots help us broadly recognize the regions where the ESR dip depth is a maximum and dip location is a minimum, as shown by the circled regions in these plots. These regions can be thought of as orientations of the NV centers in a diamond nanocrystal, where we can hope for them to behave as θ^2 sensors. For the plots shown here, in the space of polar $[0-90^\circ](\phi)$ and azimuthal $[0-360^\circ](\Theta)$ angles, these regions can be picked as follows - (a)around $50-70^\circ \phi$ and $90-120^\circ \Theta$, (b)around the pole of the hemisphere i,e, $0-20^\circ \phi$ and $250-280^\circ \Theta$ and (c)around $70-90^\circ \phi$ and $330-3520^\circ \Theta$. Due to the experimentally accessible magnetic field region being close to the pole of the hemispheres, we chose location (b) for further exploration. Fig. 5(c) shows the ESR dip at 20 mT at $12.5^\circ \phi$ and $264^\circ \Theta$ which, as theoretically expected, is shifted to ≈ 2.3 GHz.

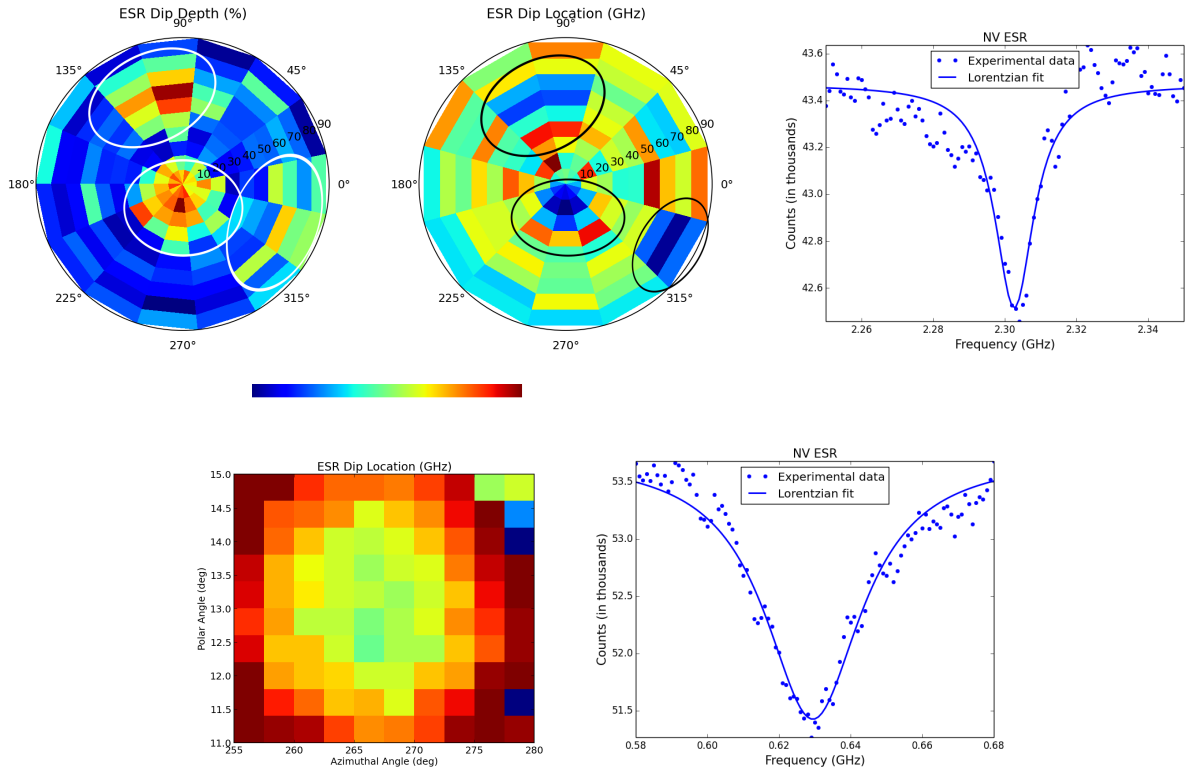


Figure 5: Trying to locate NV orientations for an arbitrarily chosen diamond nanocrystal (a)Monitoring the ESR dip depth while sweeping 20 mT B_{ext} around in azimuthal and polar angles about the $+\hat{z}$ direction and projecting the hemisphere onto a polar plot, (b)Similarly monitoring and plotting the ESR dip location. Circled regions exhibit maximum dip depth and minimum dip location, thus being plausible NV orientations., (c)Maximally shifted ESR dip at 20 mT at a location closest to the pole - $12.5^\circ \phi$ and $264^\circ \Theta$, (e)Similarly monitoring the ESR dip location at 80 mT B_{ext} and projecting the spherical cap onto a planar plot and (f)Maximally shifted ESR dip at 80 mT at the same location as above. The colormap for the projection plots is also shown.

After choosing a broad location, such as (b) for this nanodiamond, we tried to narrow down the spread of this region in both ϕ and Θ , by probing with higher magnetic fields. Fig. 5(e) shows such a plot of the behavior of the ESR dip location while sweeping 80 mT magnetic field. As can be seen in this plot, the spread of both polar and azimuthal angles narrows down as the external magnetic field is increased. A thing to note in this plot is that the spread in the polar angle direction is much finer ($<5^\circ$) than the spread in the azimuthal angle direction ($<25^\circ$), which is expected for regions around the pole. The shifted ESR dip at 80mT at $13.4^\circ \phi$ and $267^\circ \Theta$ is shown in Fig. 5(f) and, as theoretically expected, is around 0.63 GHz.

By scanning B_{ext} between 0-95 mT, and analyzing the shifting of the ESR dip in location and frequency, following trends were observed.

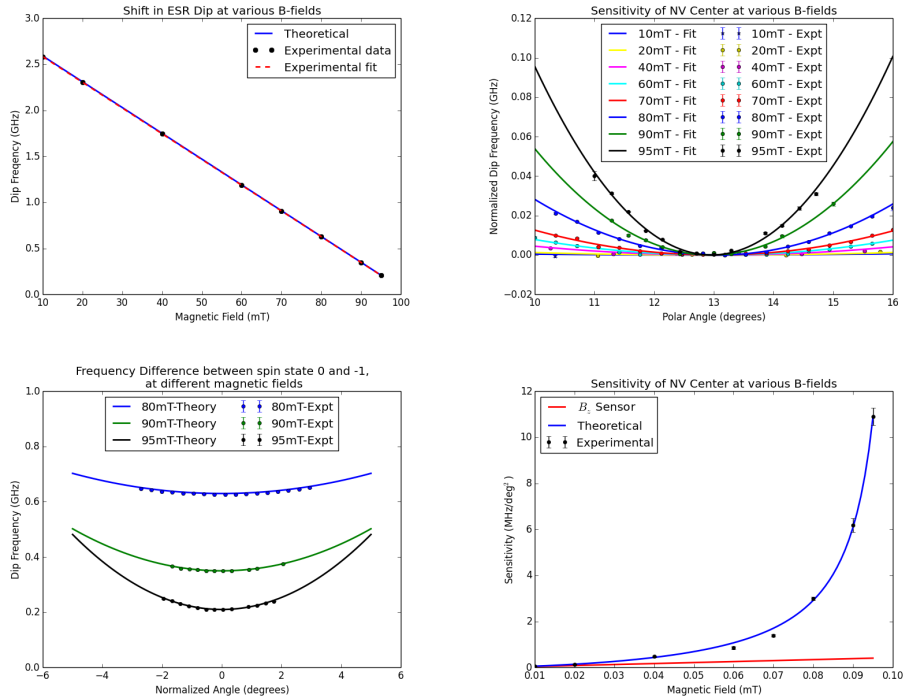


Figure 6: Various trends seen with the shift of ESR dip on applying external magnetic field (a)As theoretically expected, the ESR dip shifts down in frequency linearly with the magnetic field., (b)The ESR dip depth and location have a quadratic behavior with angle, which is plotted here with respect to the polar angle at various magnetic fields, (c)The difference in eigenvalues of $|0\rangle$ and $| -1\rangle$ spin states achieved experimentally agrees very well with the theoretical predictions and (d)Plotting the quadratic sensitivity at different magnetic fields shows that the NV center is a much more sensitive θ^2 sensor than any general naive sensor.

As seen in Fig. 6(a), the ESR dip that shifts down in frequency on increasing magnetic field does so linearly. Fitting the experimental data to a straight line, we get an x-intercept of 102.46 mT, which is very close to the expected value of B_{zfs} , and a y-intercept of 2.863 GHz,

which is very close to the expected frequency of the ESR dip without an external magnetic field. At various magnitudes of B_{ext} , we quantitatively explored the variation of the ESR dip depth and location, with respect to both ϕ and Θ angles, and found this variation to be quadratic. We explored this variation with ϕ and Θ iteratively, and for the plots presented here, we fixed the azimuthal angle at its minima (266.5° for the location (b) on this nanocrystal). This quadratic variation was expected from Eq. 3, and the variation of the ESR dip frequency (normalized for the plot's y-axis) with respect to ϕ is plotted in Fig. 6(b). The experimental data (normalized for the plot's x-axis) with the expected theoretical results is plotted in Fig. 6(c), and they seem to be in great agreement. The data presented here was fit to quadratic functions, and the coefficient of the quadratic term at different magnitudes of B_{ext} was noted as the sensitivity of measuring θ^2 at that magnetic field. These experimentally measured sensitivities are plotted in Fig. 6(d) and seem to be in great agreement with the expected theoretical behavior. This experimentally verifies that the NV centers are great θ^2 sensors, the sensitivity for which increases as B_{ext} increases, and diverges as it approaches B_{zfs} . As mentioned before, for a general magnetic field sensor, say the NV center measuring the component of the magnetic field along its axis, the sensitivity of measuring θ^2 would be linear, as shown by 'B_z Sensor' line on plot Fig. 6(d). This clearly shows that if the NV centers' axis is aligned with B_{ext} , they can work as great θ^2 sensors.

4 Conclusion

In conclusion, we have developed an experimental scheme to estimate the NV centers' axes in any arbitrarily chosen diamond nanocrystal. We further demonstrated the ability to align an external magnetic field with the direction of the NV center and sweep the external field around it in a spherical fashion. Using this technique, we have clearly shown that if the NV centers' axis is aligned with B_{ext} , they can act as very effective θ^2 sensors, the sensitivity for which increases much faster than linearly with increasing external field. This sensitivity diverges as B_{ext} approaches $B_{zfs} \approx 102.5$ mT, practically limiting the sensitivity. We have also experimentally shown that the sensitivity for this measurement matches perfectly with its theoretical predictions. The ability of the NV centers to be very sensitive θ^2 sensors demonstrates that they can be very effectively used for making QND measurements on systems such as a harmonic oscillator. This class of measurements lends use in a variety of applications such as gravity wave detection and probing quantum behavior of NMOs in a hybrid system.

References

- [1] B. D'Urso, MV Gurudev Dutt, S. Dhingra, and NM Nusran. Quantum measurements between a single spin and a torsional nanomechanical resonator. *New Journal of Physics*, 13:045002, 2011.

- [2] J.H.N. Loubser and J.A. van Wyk. Electron spin resonance in the study of diamond. *Reports on Progress in Physics*, 41(8):1201, 1978.
- [3] N.B. Manson, J.P. Harrison, and M.J. Sellars. Nitrogen-vacancy center in diamond: Model of the electronic structure and associated dynamics. *Phys. Rev. B*, 74:104303, 2006.
- [4] Marcus W Doherty, Neil B Manson, Paul Delaney, Fedor Jelezko, Jörg Wrachtrup, and Lloyd CL Hollenberg. The nitrogen-vacancy colour centre in diamond. *Physics Reports*, 528(1):1–45, 2013.
- [5] C. L. Degen. Scanning magnetic field microscope with a diamond single-spin sensor. *arxiv:cond-mat/0805.1215*, 2008.
- [6] J. M. Taylor, P. Cappellaro, L. Childress, L. Jiang, D. Budker, P. R. Hemmer, A. Yacoby, R. Walsworth, and M. D. Lukin. High-sensitivity diamond magnetometer with nanoscale resolution. *Nature Physics*, 4:810, 2008.
- [7] G. Balasubramanian, I. Y. Chan, R. Kolesov, M. Al-Hmoud, J. Tisler, C. Shin, C. Kim, A. Wojcik, P. R. Hemmer, A. Krueger, T. Hanke, A. Leitenstorfer, R. Bratschitsch, F. Jelezko, and J. Wrachtrup. Nanoscale imaging magnetometry with diamond spins under ambient conditions. *Nature*, 455:648, 2008.
- [8] J. R. Maze, P. L. Stanwix, J. S. Hodges, S. Hong, J. M. Taylor, P. Cappellaro, L. Jiang, M. V. G. Dutt, E. Togan, A. S. Zibrov, A. Yacoby, R. L. Walsworth, and M. D. Lukin. Nanoscale magnetic sensing with an individual electronic spin in diamond. *Nature*, 455:644, 2008.
- [9] Steffen Steinert, Florian Dolde, Philipp Neumann, Andrew Aird, Boris Naydenov, Gopalakrishnan Balasubramanian, Fedor Jelezko, and Joerg Wrachtrup. High sensitivity magnetic imaging using an array of spins in diamond. *Review of scientific instruments*, 81(4):043705, 2010.
- [10] Liam T Hall, Jared H Cole, Charles D Hill, and Lloyd CL Hollenberg. Sensing of fluctuating nanoscale magnetic fields using nitrogen-vacancy centers in diamond. *Physical review letters*, 103(22):220802, 2009.
- [11] D. Rugar, R. Budakian, H. J. Mamin, and B. W. Chui. Single spin detection by magnetic resonance force microscopy. *Nature*, 430:329, 2004.
- [12] Olivier Arcizet, Vincent Jacques, Alessandro Siria, Philippe Poncharal, Pascal Vincent, and Signe Seidelin. A single nitrogen-vacancy defect coupled to a nanomechanical oscillator. *Nature Physics*, 7(11):879–883, 2011.
- [13] V. B. Braginsky, Y. I. Vorontsov, and K. S. Thorne. Quantum nondemolition measurements. *Science*, 209:547, 1980.

- [14] C. M. Caves, K. S. Thorne, R. W. P. Drever, V. D. Sandberg, and M. Zimmermann. On the measurement of a weak classical force coupled to a quantum-mechanical oscillator. I. Issues of principle. *Rev. Mod. Phys.*, 52:341, 1980.
- [15] A Brillet, T Damour, and Ph Tourrenc. Introduction to gravitational wave research. In *Annales de Physique*, volume 10, pages 201–218. Les Editions de Physique, 1985.
- [16] M. F. Bocko and R. Onofrio. On the measurement of a weak classical force coupled to a harmonic oscillator: experimental progress. *Rev. Mod. Phys.*, 68:755, 1996.
- [17] Philippe Grangier, Juan Ariel Levenson, and Jean-Philippe Poizat. Quantum non-demolition measurements in optics. *Nature*, 396(6711):537–542, 1998.
- [18] J. Wrachtrup and F. Jelezko. Quantum information processing in diamond. *J. Phys.: Condens. Matter*, 18:S807, 2006.
- [19] A. Gruber, A. Drabenstedt, C. Tietz, L. Fleury, J. Wrachtrup, and C. von Borczyskowski. Scanning confocal optical microscopy and magnetic resonance on single defect centers. *Science*, 276:2012, 1997.